PCCP

Accepted Manuscript

This article can be cited before page numbers have been issued, to do this please use: Z. Liu, V. S. Nguyen, J. Harvey, J. Muller and J. Peeters, *Phys. Chem. Chem. Phys.*, 2017, DOI: 10.1039/C7CP00288B.

ROYAL SOCIETY OF CHEMISTRY

rsc.li/pccp

View Article Online
DOI: 10.1039/C7CP00288B

PCCP

ARTICLE

Theoretically Derived Mechanisms of HPALD Photolysis in Isoprene Oxidation

Received 00th January 2017,
Accepted 00th January 2017

DOI: 10.1039/x0xx00000x

www.rsc.org/

Zhen Liu[a], Vinh Son Nguyen[a], Jeremy Harvey[a], Jean-François Müller[b], and Jozef Peeters[a*]

In this work we identified and theoretically quantified two photolysis mechanisms of HPALDs (hydroperoxy aldehydes) that result from the isomerization of peroxy radicals in the atmospheric oxidation of isoprene at low/moderate NO_x. As a first photolysis mechanism, we show that a fraction of the initially excited S_1-state HPALDs isomerizes by a near-barrierless 1,5 H-shift at a rate approaching 10^{12} s^{-1} — competing with the ~equally fast intersystem crossing to the T_2 triplet state — forming an unstable biradical that spontaneously expels an OH (hydroxyl) radical. A second mechanism is shown to proceed through the activated T_2 triplet biradical — formed from S_1 — undergoing a concerted ring-closure and OH-expulsion, yielding an oxiranyl-type co-product radical that quickly ring-opens to enoxy radicals. In both mechanisms, subsequent chemistry of the co-product radicals yields additional first-generation OH. The combined HPALD-photolysis quantum yield by these two mechanisms — which may not be the only photolysis routes— is estimated at 0.55 and the quantum yield of OH generation at 0.9, in fair accord with experimental data on an HPALD proxy (Wolfe et al., PCCP, 2012, **14**, 7276-7286.).

Introduction

Terrestrial vegetation releases vast amounts of volatile organic compounds (VOCs), among which isoprene is by far the most important, with global annual emissions of *ca*. 500 Tg.[1] Its rapid oxidation in the atmosphere affects air quality and climate through effects on ozone, particulate matter and the hydroxyl radical (OH) which, as the main oxidizing agent in the atmosphere, controls the lifetime of numerous pollutants. Motivated by the apparent failure of models to match the high OH abundance reported in isoprene-rich areas under low-NO_x conditions,[2,3] theoretical and experimental investigations[4-9] challenged the prevailing assumptions and led to a considerably more complex view of the oxidation mechanism of isoprene and other VOCs, in which the loss of OH incurred by its reaction with a VOC is partly compensated by substantial OH re-formation in subsequent reactions of the oxidized reaction products. Such OH recycling mechanisms dampen the sensitivity of OH to perturbations associated with emission changes, thereby contributing to the stability of global OH levels.[10]

The present study builds on our previous theoretical investigations of the isoprene oxidation mechanism (Leuven Isoprene Mechanism, LIM), focusing in particular on previously unsuspected unimolecular reactions of isoprene hydroxyperoxy radicals (ISOPO2) formed from the successive addition of OH and O_2 to isoprene.[4,8,11] Possibly the most important OH recycling mechanism associated to VOC chemistry is indeed the isomerization through 1,6-H shift of specific ISOPO2 radicals, the *Z*- δ-hydroxy-isoprenyl-peroxy radicals, leading to the formation of a hydroperoxy radical (HO_2) along with a photolabile hydroperoxyenal (HPALD) of which the fast photodissociation into OH and an enoxy radical was proposed to be a significant secondary source of OH.[4,11] Fast HPALD photolysis follows from high absorption cross sections (comparable to the known cross sections of similar enals such as methacrolein) and a photolysis

[a] *Department of Chemistry, University of Leuven, Celestijnenlaan 200F, B-3001 Leuven, Belgium.*
[b] *Royal Belgian Institute for Space Aeronomy, Avenue Circulaire 3, B-1180 Brussels, Belgium.*
*Email: Jozef.Peeters@kuleuven.be
Electronic Supplementary Information (ESI) available. Geometries and Cartesian coordinates, See DOI: 10.1039/x0xx00000x

quantum yield (QY) estimated to be close to unity, as confirmed by the high QY (1 ± 0.4) derived experimentally for the HPALD proxy *Z*- O=CH-CH=CH-CH(OOH)C_2H_5.[12] Furthermore, the experimental OH quantum yield (1 ± 0.8) suggests that OH dissociation is the dominant pathway, as predicted for the isoprene-derived HPALDs.

Formation of HPALD in isoprene oxidation was observed in the laboratory by Crounse et al.[13] at yields much lower than our original predictions[11] but in reasonable agreement with our higher-level theoretical appraisal,[8] when considering the respective uncertainties and acknowledging the identification of an additional isomerization pathway of the *Z*- δ-hydroxy-isoprenyl-peroxy radicals, theoretically estimated to be of importance comparable to the HPALD route.[8] HPALDs were also measured in the lower troposphere over the Southeastern U.S. during the SEAC[4]RS aircraft campaign,[14] with average near-surface concentrations of ~100 ppt, i.e. about half the average levels of isoprene hydroxyhydroperoxides (ISOPOOH). Using the Geos-Chem global model, with HPALD-formation rates from Crounse et al., Travis et al.[14] estimated that HPALD formation represented *ca*. 15% of the total ISOPO2 sink on global average. Note that in spite of this sizeable contribution, when assuming fast HPALD photolysis as described above (QY=1), the model underestimated the SEAC[4]RS HPALD measurements by a factor of 2 (whereas ISOPOOH levels were overestimated), suggesting a possible imbalance in the global HPALD budget.

The photolysis of HPALD was originally proposed[4,11] to proceed by the avoided crossing of the excited state of the enone chromophore (S_1 or T_1) with the repulsive excited state of the hydroperoxide chromophore (S_2 or associated triplet), resulting in dissociation into OH and an enoxy radical which was proposed to undergo a sequence of fast reactions leading eventually to photolabile peroxyacyl aldehydes (PACALDs). However, we later identified a faster photolysis mechanism[8] resulting in higher estimated internal energy in the oxy radicals, and therefore to a different subsequent chemistry.

In this work, we aim to fully elucidate, at higher levels of theory, the detailed sequence of reactions of the fast photolysis route(s), starting from the initially excited HPALD, that leads to its dissociation and to the eventual formation of first-generation hydroxyl radicals, both in a primary step and in subsequent radical chemistry.

Methodologies

For all the ground state molecules studied here, a molecular mechanics (MM) conformational analysis was first performed with the Tinker program.[15] A suitable MM atom type was assigned to each atom based on the MMFF force field definition. For the TS structures, a modified atom type was adopted so as to keep the connectivity and bond lengths close to those of the target TS structure. For instance, H atom transferring from an atom X to an atom Y was replaced with O atom. All the initial structures obtained at the MM level were then optimized at M06-2X-D3/6-311++G(2d,p) level using Gaussian 09.[16] For the lowest-energy conformers, the structure was reoptimized and frequencies calculated at the same level of theory, but with tight geometry convergence criteria and superfine density functional theory integration grids in order to minimize numerical error for the vibrational frequencies. Single-point CCSD(T)-F12b energies were computed with the Molpro 2012.1 program,[17] using the cc-pVDZ-F12 basis set for the orbitals, the def2-QZVPP basis set for the density fitting, and the def2-TZVPP basis set as the complementary auxiliary basis set. A restricted HF-reference wavefunction was used for the coupled cluster calculations on closed-shell molecules (RHF/CCSD(T)), while a restricted open-shell HF-reference wavefunction was adopted for the unrestricted coupled cluster calculations on open-shell molecules (ROHF/UCCSD(T)). Unless mentioned otherwise, all reported energies on the PES are the CCSD(T)-F12/cc-pVDZ-F12 calculations with ZPVE corrections from M06-2X-D3/6-311++G(2d,p), on the basis of the lowest conformers of the reactant and the transition state.

The electronically-excited S_1 state of *Z*- HPALD(II), and the corresponding transition state for 1,5 H-shift, were studied using four different functionals M06, M06-2X, wB97XD, and Cam-B3LYP by adopting the time-dependent DFT approach (TDDFT), as implemented in Gaussian 09.[16] In each case, the structure was optimized and frequencies calculated at the TDDFT level; relative energies are given with respect to the ground state structure obtained using the same functional and basis set.

The statistical-kinetics rates were derived using Transition State Theory (TST) for thermal unimolecular reactions and RRKM theory for chemically activated reactions.[18,19] For a number of important thermal reactions, with several low-lying rotameric conformers of the reactant and of the transition state, separated by conformational isomerization barriers of 3-12 kcal mol^{-1}, Multi-Conformer Transition State Theory (MC-TST) was applied.[20] In all cases, thermal rate coefficients were evaluated from the free energies provided by Gaussian 09, based on the unscaled M06-2X vibrational frequencies and rigid-rotor constants detailed above. It was ascertained for some of the unimolecular reactions that the M06-2X frequency-scaling by 0.97 has a negligible effect, far below the error margin due to the uncertainties on the (free) energies. The tunnelling factors, sometimes very high for hydrogen-shift reactions, were estimated assuming an asymmetric Eckart potential[21,22] and using the M06-2X calculated frequencies (see above).

The implementation of the Multi-Conformer RRKM approach for chemically activated reactions, in terms of the sum of accessible states $G^{\neq}(E_v - E^{\neq})$ of the transition state conformers and the density of states of the reactant conformers $N(E_v)$, is detailed in the Results and Discussion section for the appropriate, major case. Here we merely give the traditional RRKM equation for the micro-canonical rate coefficient:

$$k(E_v) = \alpha \times G^{\neq}(E_v - E^{\neq}) / (h \times N(E_v))$$

in which α is the reaction path degeneracy, h Planck's constant, $E^{\neq}$ the TS energy, E_v the vibrational energy of the reacting activated intermediate, $N(E_v)$ its density of vibrational states, and $G^{\neq}(E_v\text{-}E^{\neq})$ the sum of accessible vibration states of the TS; both the latter were evaluated by exact count.[19] For the principal activated reactions, the rate was integrated over the energy distribution function of formation $F(E_v)$; for cases where the distribution is narrow and the exact value of the rate is not important by lack of real competition, the rates were estimated at the average energy.

Regarding the competition between collisional stabilization and reaction of the lowest triplet T_2 state of HPALDs (see Results section), the Lennard-Jones collision frequency of T_2 with air molecules, $k_{coll} = Z_{LJ}[M]$, was estimated[23] to be about 1.3×10^{10} s^{-1} at 298 K and 1 atm, while the average energy transferred per collision was assumed to be $\langle \Delta E \rangle_{all} = -200$ cm^{-1}. As expected for this case where stabilization requires several tens of collisions, it was found that for a given $\langle \Delta E \rangle_{all}$, the bi-exponential energy transfer model of Troe[24], implemented in a quasi-stochastic approach, led to nearly the same result as a fixed energy transfer per collision.

Results and Discussion

As HPALD(II) is found to be by far the most important HPALD from isoprene at low/moderate NO,[25] the present theoretical work is focused on this compound; when mechanistic aspects for HPALD(I) differ in a major way, this will be mentioned explicitly. HPALDs from isoprene are produced solely as the *Z*- isomers. For the S_0 ground state of HPALD(II), the lowest conformer of the *Z*- isomer has nearly the same potential energy as the lowest conformer of the *E*-isomer, whereas the lowest *Z*-HPALD(I) lies 2.4 kcal mol^{-1} above its *E*- counterpart. As the UV-Vis absorption spectrum for the $S_0 \rightarrow S_1$ transition of HPALDs is not known, the well–established spectrum of the enal template molecule methacrolein (MACR) is adopted here as a proxy. The chromophore in both molecules is the conjugated enal frame O=C-C=C. It was verified at the time-dependent density functional theory level TD-M062x-GD3/6-311++G that the adiabatic $S_0 \rightarrow S_1$ excitation energy for MACR and HPALD II, of 77.7 and 78.8 kcal mol^{-1} respectively, are very similar, which supports our use of the MACR spectrum as a proxy. The $S_0 \rightarrow S_1$ excitation energy distribution function $F(E_{exc})$ of the *Z*-HPALDs I and II is obtained as the product of the MACR absorption cross section[26] and the actinic photon flux at the earth's surface for an overhead sun,[27] both as functions of wavelength, convoluted with the thermal vibrational energy distribution of S_0 at 298 K derived from the computed vibrational frequencies. The average vibrational energy of the ground state is close to 4.0 kcal mol^{-1}. The resulting smoothed $F(E_{exc})$ function, depicted in the ESI (Figure S1), shows a FWHM width close to 15 kcal mol^{-1} with a maximum at 89 kcal mol^{-1}, which is also the median E_{exc}.

Photolysis mechanism of the HPALD S_1 state. A first mechanism of HPALD photolysis, involving the S_1 excited state **1** is schematically presented in the potential energy

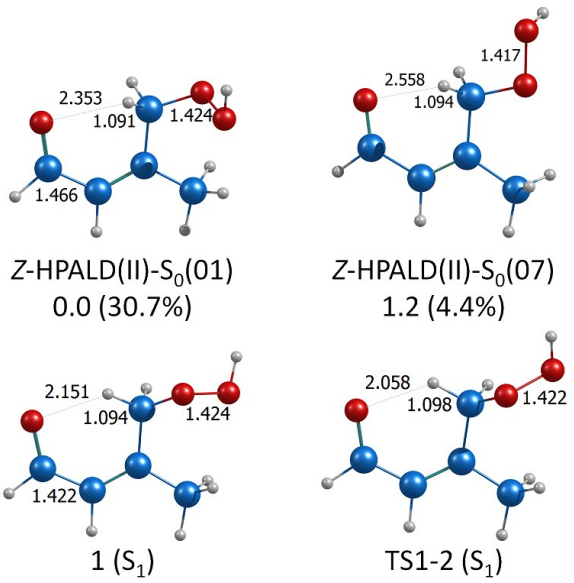

Figure 2. Structures of two singlet *Z*- HPALD(II) conformers that can undergo direct 1,5-H shift after excitation, of the excited-state S_1 geometry, and of the transition state for 1,5-H shift on the S_1 surface, optimized at M06-2X-D3/6-311++G(2d,p) level of theory and at TD-M06-2X-D3/6-311++G(2d,p) level of theory for the excited state. All 13 conformers of *Z*- HPALD(II) are depicted in the ESI (Figure S3).

surfaces of Figures 1a and 1b, while the energy and free energy (298 K) data at two levels of theory are listed in Table 1. The structures of the lowest-energy conformers of all minima and transition states involved in this mechanism are depicted in the ESI (Figure S2). Thirteen rotameric conformers of the S_0 ground state were identified, shown in the ESI (Figure S3) together with their computed relative free energies *G*(298 K) and fractional Boltzmann populations at 298 K. The lowest-energy conformer and one other conformer, accounting together for 35% of the population, have the carbonyl-O atom pointing inwards, which, once excited to the S_1 state, allows formation of a non-classical, ≈4 kcal mol^{-1} strong hydrogen bond, as shown in Figure 2. The TD-DFT computed relative energies of the S_1 conformer resulting from the lowest S_0 rotamer, of 73.3, 76.7, 78.3 and 79.2 kcal mol^{-1}, for DFT = M06, M06-2X, wB97XD, and Cam-B3LYP, respectively, compare reasonably with the experimental acrolein S_1 energy of 74 kcal mol^{-1}.[28] For acrolein, the S_1 surface is known to be intersected close to its minimum by the surface of the twisted triplet T_2 state[29] such that S_1 undergoes very fast intersystem crossing (ISC) to T_2, at a rate measured to be 5 × 10^{11} s^{-1} by Paulisse et al..[30] We assume that *Z*- HPALD(II)-**1**(S_1) similarly crosses rapidly to triplet T_2 on a timescale of 2 ps. However, the specific **1**(S_1) conformers above can undergo a very fast 1,5 H-shift of the hydrogen-bonded H to the carbonyl-O radical site. The barrier height for this shift for the most abundant conformer, computed using the four TD-DFT methods above, was found to be only −0.4, 0.7, −0.1 and −0.2 kcal mol^{-1}, respectively, likely owing to the pre-reactive H-bond. Adopting a conservative estimate of 1 kcal mol^{-1} for the barrier height, the RRKM-calculated rate at the average energy of some 10 - 15 kcal mol^{-1} is (4 to 9) × 10^{11} s^{-1}, similar to the expected ISC rate. It may be noted that the microcanonical rate coefficient for the 1,5 H-shift already levels off at the average energy to its asymptotic limit and therefore does not depend overly on the initial excitation energy, as shown in Table S2. At the same time, it can be expected that the rates of both the H-shift and the ISC increase similarly with energy. On the other hand, the hydrogen bond, together with the partial double bond between the carbonyl-C and its neighbour (see Figure 2) owing to delocalization of the π-system of S_1 preempts fast internal rotation and conversion to other S_1 conformers, most of which have the carbonyl-O pointing outwards. Thus, an estimated 20 ± 4% of the excited HPALD(II) is expected to follow the H-shift route; the stated uncertainty reflects only the expected error on the 1,5 H-shift rate. For HPALD(I) this percentage is *ca.* 13 ± 4% because of lower thermal populations of the S_0 conformers that can result in the 1,5 H-shift when excited to the S_1 state. It may be noted that internal conversion of S_1 to vibrationally excited S_0 — which could be followed by impulsive decomposition into OH and an enoxy radical — can only become competitive with the very fast ISC to T_2 at much higher excitation energies than those at hand.[29,31]

The 1,5 H-shift in the specific conformers of **1**(S_1) yields the activated α-hydroperoxy-biradical **2**, which, similar to α-hydroperoxy alk(en)yl radicals,[32] should be unstable and spontaneously expel OH to form a carbonyl doublet radical **3** as shown in Figure 1a. For better precision, the transition state **TS1-2** to this concerted process was computed for the triplet counterpart of **2** —

View Article Online
DOI: 10.1039/C7CP00288B

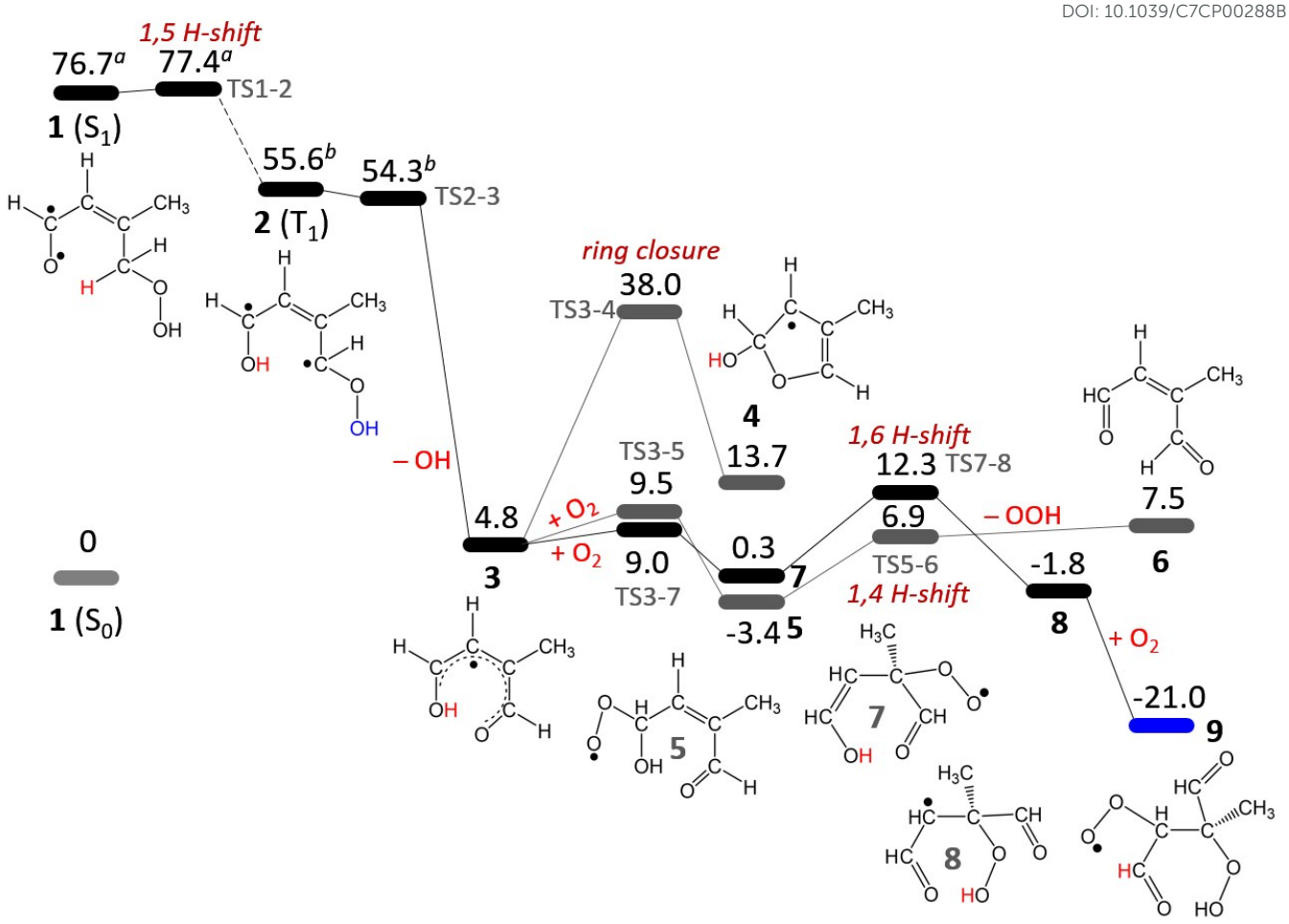

Figure 1a. Potential energy surface for the reactions of the excited HPALD(II) through the triplet (T_1) state. Coupled-cluster energies (kcal mol^{-1}) relative to the global minimum singlet *Z*- HPALD(II) and the corresponding fragments OH, OOH and O_2, based on DFT geometries (CCSD(T)-F12/cc-pVDZ-F12//M06-2X-D3/6-311++G(2d,p) level of theory). ZPVE at M06-2X-D3/6-311++G(2d,p) level is included. [a] For the excited **1** and **TS1-2**, the TD-M06-2X-D3 energies are shown. [b] Energies computed for the corresponding triplet state, see text. All structures are depicted in the ESI (Figure S2).

which should be structurally and energetically very similar to the singlet biradical — and, at the CCSD(T) level of theory, the reaction was indeed found to be a nearly barrierless reaction. Thus, OH is formed here from **1**(S_1) in a sequence of two near-barrier-free, very fast steps on a time scale of ~1 ps. The by far lowest-energy conformer (out of 15) of the co-product radical **3** (see Figure 1a and Table 1) is strongly stabilized by two resonances and by a 17 kcal mol^{-1}, unusually strong H-bond, affording this doublet radical semi-aromatic character. It is expected to contain some 50 - 70 kcal mol^{-1} internal energy after OH expulsion, and may undergo two prompt unimolecular reactions, but even the fastest one — shown in Figure 1a — faces a barrier of 33.2 kcal mol^{-1} such that at most 20% of the initially activated **3** can escape collisional stabilization, its by far dominant fate. The prevailing reaction of **3** is therefore O_2-addition after stabilization. However, very different from known O_2 additions to other organic radicals, the O_2-additions to the two possible radical-sites of **3** to form the peroxys **5** and **7** (with two enantiomers each) face potential energy barriers of 4.7 and 4.2 kcal mol^{-1}, respectively, each through a single low-lying transition state that in addition is quite tight, resulting in unusually low bimolecular rate coefficients at 298 K of k(3,5) = 5.9× 10^{-17} and k(3,7) = 1.38 × 10^{-17} cm^3 molecule^{-1} s^{-1}. In the lower atmosphere, at [O_2] of ~5 × 10^{18} cm^{-3}, this implies first-order removal rates of **3** of only 100 s^{-1}, which is 5 orders of magnitude lower than

View Article Online
DOI: 10.1039/C7CP00288B

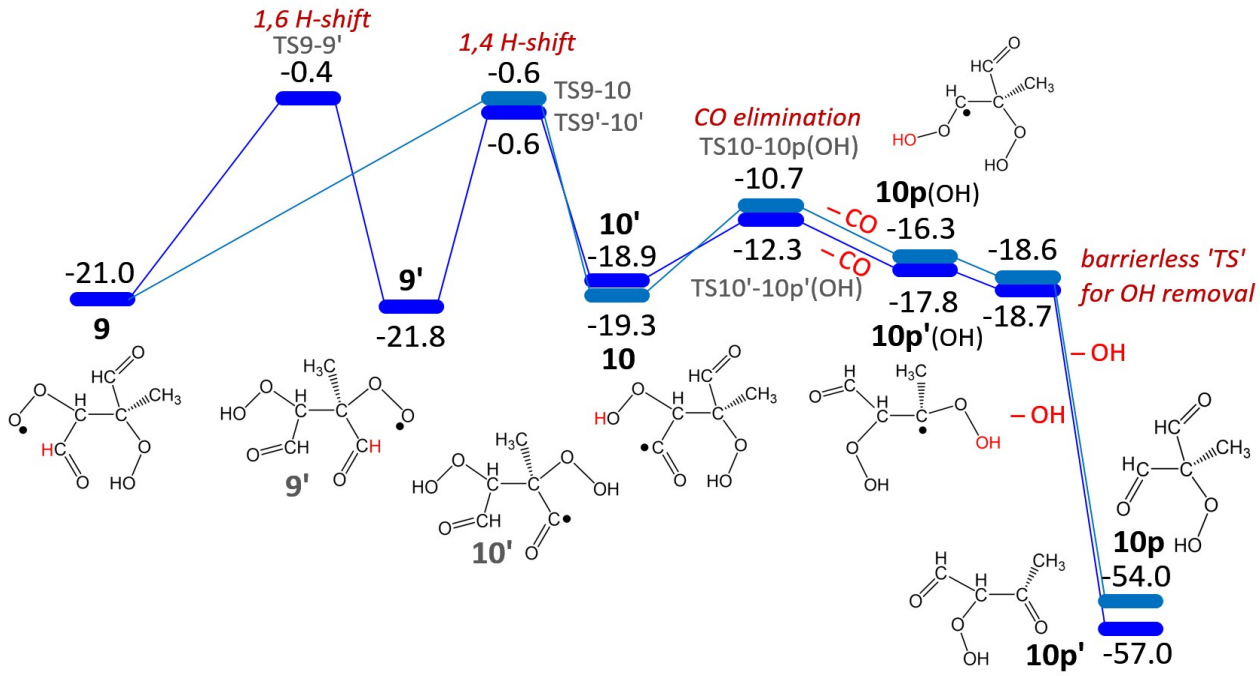

Figure 1b. Potential energy surface for the reactions of the excited HPALD(II) through the triplet (T_1) state. Coupled-cluster energies (kcal mol^{-1}) relative to the global minimum singlet *Z*- HPALD(II) and the corresponding fragments OH, OOH and O_2, based on DFT geometries (CCSD(T)-F12/cc-pVDZ-F12//M06-2X-D3/6-311++G(2d,p) level of theory). ZPVE at M06-2X-D3/6-311++G(2d,p) level is included. All structures are depicted in the ESI (Figure S2).

the usual loss rates of organic radicals by O_2-addition. As a result of the exceptional stability of the **3** radical, the two O_2-addition channels are exothermic by only 8.2 and 4.3 kcal mol^{-1}, respectively — well below the usual 20 - 40 kcal mol^{-1} for organic radicals — entailing that the thermal redissociation of the labile peroxy products can be quite important. Nevertheless, O_2 addition should be the principal if not only thermal atmospheric reaction of this unusual and poorly reactive **3** radical.

The predicted ratio of formation of the peroxy species **7** and **5**, obtained from the $\Delta G^{\neq}$ between the lowest conformer of **3** and the associated TSs, is calculated to be k(3,7)/k(3,5) = 2.33 : 1. For these peroxys, respectively 59 and 77 conformers have been characterized. Peroxy **5** undergoes fast HO_2 elimination over a rate-limiting energy barrier of 10.3 kcal mol^{-1} through a post-reactive complex (not shown in Figure 2), yielding 2-methyl-butenedial, **6**. The rate constant of this reaction at 1.73 × 10^5 s^{-1} is over 200 times faster than that for redissociation into O_2 + **3** at 7.8 × 10^2 s^{-1} (for both considering only the lowest conformer of **5**) such that only the step **3** + O_2 to **5** determines the formation rate of HO_2 + 2-methyl-butenedial. The atmospheric fate of the latter is controlled almost uniquely by its very fast photolysis at rate ~2 × 10^{-3} s^{-1} with a β-oxoketene as principal product and only minor radical production.[33]

Matters are different for the second product route of **3**, through peroxy **7**, with redissociation at 8.4 × 10^6 s^{-1} effectively competing with its 1,6 H-shift to yield **8** with rate constant 7.3 × 10^6 s^{-1}, the latter accounting for the high asymmetric-Eckart tunneling factor of 1200 for an imaginary TS-frequency of 2450i cm^{-1} and including a contribution of a second TS lying 0.9 kcal mol^{-1} above the lowest (increasing the rate constant by a factor 1.22). From these rate data and the k(3,7)/k(3,5) ratio of 2.33 above, it follows that the net branching ratio of the **3** reaction pathways to **8** and **6** is 1.08 : 1. Note that to derive this ratio, the various conformers and associated energies of **5** and **7** do not have to be known, as for both radicals only the ratios of the two competing reactions come into play. The barrier faced by the enolic 1,6 H-shift of **7** to form **8**, of only 12.0 kcal mol^{-1}, is in keeping with

View Article Online
DOI: 10.1039/C7CP00288B

Table 1: Relative energies and free energies (kcal mol^{-1}) at 298 K for the structures in Figure 1a and Figure 1b.

	$\nu_{im}^{\neq}$/i	ΔE_1	ΔG_1 (298 K)	ΔE_2	ΔG_2 (298 K)
1 (S_1)		76.7	76.4	-	-
TS1-2	-63	77.4	77.7	-	-
2 (T_1)		54.3	53.1	55.6	54.3
TS2-3	-552	54.8	53.6	54.3	53.1
3		3.0	-6.4	4.8	-4.6
TS3-4	-558	38.5	29.6	38.0	29.0
4		14.7	5.5	13.7	4.4
TS3-5	-587	12.9	13.8	9.5	10.3
5		-2.7	-2.5	-3.4	-3.2
TS5-6	-793	8.5	8.7	6.9	7.0
6		11.3	0.4	7.5	-3.4
TS3-7	-562	12.5	13.4	9.0	9.8
7		0.2	1.7	0.3	1.8
TS7-8	-2518	13.4	15.3	12.3	14.2
8		-1.7	-0.5	-1.8	-0.6
9		-21.3	-9.2	-21.0	-8.8
TS9-10	-1926	1.5	14.0	-0.6	12.0
10		-18.9	-6.7	-19.3	-7.1
TS10-10p(OH)	-321	-11.3	0.3	-10.7	0.8
10p(OH)		-15.4	-13.4	-16.3	-14.3
TS9-9’	-4464	0.9	13.6	-0.4	12.3
9’		-22.5	-10.4	-21.8	-9.7
TS9’-10’	-1881	1.4	13.4	-0.6	11.3
10’		-19.5	-7.2	-18.9	-6.6
TS10’-10p’(OH)	-316	-12.7	-1.7	-12.3	-1.4
10p’(OH)		-14.5	-13.6	-17.8	-16.8
10p		-48.8	-56.4	-54.0	-61.6
10p’		-52.7	-60.6	-57.0	-64.9

ΔE_1, the relative energy with inclusion of ZPVE at M06-2X-D3/6-311++G(2d,p) level of theory; ΔG_1, the relative Gibbs free energy (298 K) at M06-2X-D3/6-311++G(2d,p) level of theory; ΔE_2, the relative energy with inclusion of ZPVE at CCSD(T)-F12/cc-pVDZ-F12//M06-2X-D3/6-311++G(2d,p) level of theory; ΔG_2, the relative Gibbs free energy (298 K) at CCSD(T)-F12/cc-pVDZ-F12//M06-2X-D3/6-311++G(2d,p) level of theory. $\nu_{im}^{\neq}$/i, the imaginary frequency of the TSs.

our earlier finding that the concerted switch of a C=C to a C=O double bond for such enolic H-shifts strongly reduces the barrier.[34]

The resulting radical **8** (with 12 characterized rotamers) will rapidly add O_2 yielding the peroxy radical **9** (with 134 conformers), a reaction that is exothermic by 19.2 kcal mol^{-1}. An expected fate of **9** is a 1,4 shift of the formyl-H to the peroxy function facing a barrier of 20.4 kcal mol^{-1}, a well-characterized type of peroxy H-shift,[6,35,36] forming here the acyl radical **10**. The imaginary frequency of the **TS9-10** is 1890i cm^{-1}, resulting in an Eckart tunneling factor κ(298 K) = 377. Considering all conformers within 1 kcal mol^{-1} of the lowest for both **9** and **TS9-10**, the thermal rate coefficient is found to be k(9,10) = 1.6 s^{-1}. An alternative 1,5 H-shift of the other formyl-hydrogen in **9**, facing a barrier that is 2.8 kcal mol^{-1} higher than the 1,4 H-shift and with a similar $\nu_{im}^{\neq}$, is negligibly slow compared to the 1,4 H-shift. However, in agreement with Jorgensen et al.,[37] a 1,6 H-shift of the hydroperoxide-H to the peroxy function to yield **9’** is much faster, even though its barrier is slightly higher than that of the 1,4 H-shift (see Figure 1b). The imaginary frequency of **TS9-9’** and hence the tunneling factor is found to be so high ($\kappa \geq 10^5$) that it outruns the 1,4 H-shift **9** → **10** by several orders of magnitude, resulting in a fast pre-equilibrium **9** ↔ **9’** in a ratio 1 : 4.6 at 298 K. The peroxy **9’** undergoes a similar 1,4 H-shift as **9**, yielding acyl radical **10’**, though with a slightly lower calculated rate k(9’,10’) of 1.2 s^{-1}, here also considering all conformers of **9’** and the TS within 1 kcal mol^{-1} of the lowest. Even allowing for the uncertainties on k(9,10) and k(9’,10’), it is clear that both 1,4 H-shifts should readily outrun the traditional peroxy reactions with NO and HO_2 under the conditions where HPALD formation from isoprene is important. The nascent acyl radicals **10** and **10’** arising predominantly by tunneling from the 1,4 H-shifts contain an average internal energy of *ca*. 15-16 kcal mol^{-1}. They promptly eliminate CO over low barriers of 8.6 and 6.6 kcal mol^{-1} at computed rates of ≈1.3 × 10^9 and ≈9.7 × 10^{10}s^{-1}, respectively. The roughly 50% of **10** that collisionally stabilizes will thermally eliminate CO at a rate still as high as 1.0 × 10^7 s^{-1}, about half as fast as atmospheric O_2 addition, such that only about a third of **10** finally adds O_2. Regarding **10’**, the already negligible fraction that survives the rapid prompt CO elimination will thermally expel CO at a rate of 4.9 × 10^8 s^{-1}, leaving none to add O_2. Overall, of **9** and **9’** nearly 95% finally results in CO elimination, yielding unstable α-hydroperoxy-alkyl-type radicals (**10p**(OH) and **10p’**(OH) in Figure 1b) that spontaneously, without barrier expel OH[32] to yield 0.15 **10p** (2-hydroperoxy-2-methyl-butanedial) and 0.78 **10p’**

View Article Online
DOI: 10.1039/C7CP00288B

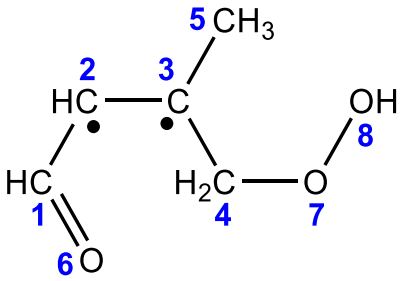

Scheme 1. Atom sequence of HPALD(II) (T_2)

(2-hydroperoxy-3-methyl-butanedial), respectively. It may be noted that the DFT functional BP86 even predicts that the acyls **10** and **10'** expel CO and OH in a concerted fashion. A similar though less complex mechanism regenerating OH and yielding hydroxyacetone has been experimentally observed by Crounse et al.[6] in the OH-initiated oxidation of methacrolein. The first-generation OH quantum yield from HPALD photolysis through the "direct" S_1 mechanism is therefore estimated at 0.3 ± 0.06. Both the hydroperoxy-dials produced from the peroxys **9** and **9'** can be expected to subsequently photolyze rapidly to yield an additional OH at a rate of order 2.5×10^{-4} s^{-1} for an overhead sun as suggested by results of Praske et al.[7] on an hydroperoxy-carbonyl, i.e. much faster than the $(0.35\text{-}0.7) \times 10^{-4}$ s^{-1} of the reaction with OH at [OH] = $(1\text{-}2) \times 10^6$ cm^{-3}.

HPALD Photolysis mechanism through the T_2 state. A second mechanism of HPALD photolysis, involving the T_2 state, is schematized in the PESs of Figures 3a and 3b, while the energies of the relevant minima and transition states are listed in Table 2; the structure of the lowest-energy conformers of all the T_2 minima are depicted in the ESI (Figure S4) and all the transition states are graphically shown in the ESI (Figure S5). The ≈80% of the S_1 not undergoing the 1,5 H-shift should convert quickly to the triplet T_2 (π, π*) state. It is denoted "T_2" because upon vertical excitation from S_0, it lies above the T_1 (n, π*) state associated with S_1 (n, π*); however, adiabatically, the lowest T_2 (π, π*) conformer has a relative energy computed at 55.0 kcal mol^{-1}, well below the T_1 state minimum, which is a similar situation to that occurs with to acrolein.[29,31] The T_2 state is an O6=C1H-C2•H-C3•(C5H_3)-C4H_2-O7O8H triplet biradical, though the lowest conformer features an H-bond between the hydroperoxide-H and the carbonyl-O6. In total the T_2 counts 29 conformers (see Figure S4, ESI), of which the most populated one at total energy 89 kcal mol^{-1} is an open *Entgegen* structure with the carbonyl-O pointing inwards and the hydroperoxide moiety outwards as indicated in Scheme 1 with the atoms numbered.

For this T_2 biradical, with an average internal energy content of 28 – 34 kcal mol^{-1}, a concerted reaction was newly identified and characterized: simultaneous formation of a new O7-C3 bond and breaking of the weak O7-O8H hydroperoxide bond, as shown in Figure 3a and Scheme 1, resulting initially in a product complex of an OH radical H-bonded to the O7 atom of the substituted, 3-membered oxirane product radical, denoted **11***E* and **11***Z*. The barrier to this reaction for the most-populated, non-H-bonded T_2 conformer is 12.1 kcal mol^{-1}. The 29 conformers of T_2 that were characterized (see Figure S4, ESI) are separated by barriers of *ca*. 10, 10, 2.5, 6 and 5 kcal mol^{-1} to internal rotation about the dihedral angles O6C1−C2C3, C1C2−C3C4, C2C3−C4O7, C3C4−O7O8 and C4O7−O8H, respectively. Three conformers feature a hydrogen bond between O6 and the hydroperoxide-H, of which two are the lowest-energy conformers, but at an internal energy of some 28-34 kcal mol^{-1}, they are not the most populated conformers owing to their higher rigidity and hence lower density of vibrational states. Of the 29, only 12 can directly undergo the concerted reaction to form the OH—**11** complex: those with the C3-C4-O7-O8 atoms in one plane and with the C3C4−O7O8 dihedral angle close to 180°, such that the half-occupied π-orbital on C3 can overlap with the elongating O7-O8 σ-orbital when this bond weakens while the C3C4O7 angle is reduced.

In total, eight transition state conformers were identified (see Figure S5, ESI), of which two are connected each to two different T_2 conformers and one even to three T_2 conformers. On account of their high internal energy around 30 kcal mol^{-1}, the 29 conformers $\mathbf{1}(T_2)_i$ can interconvert quickly to the 12 "reactive" conformers $\mathbf{1}(T_2)_j$ over low barriers of only 2 – 6 kcal mol, much faster than the $\mathbf{1}(T_2)_j$ conformers react to OH + **11** over the barrier of 12 kcal mol^{-1}, such that the 29 conformers should remain in approximate microcanonical equilibrium. As a result, the relative populations P_i at internal energy E will be proportional to their respective densities of vibrational

View Article Online
DOI: 10.1039/C7CP00288B

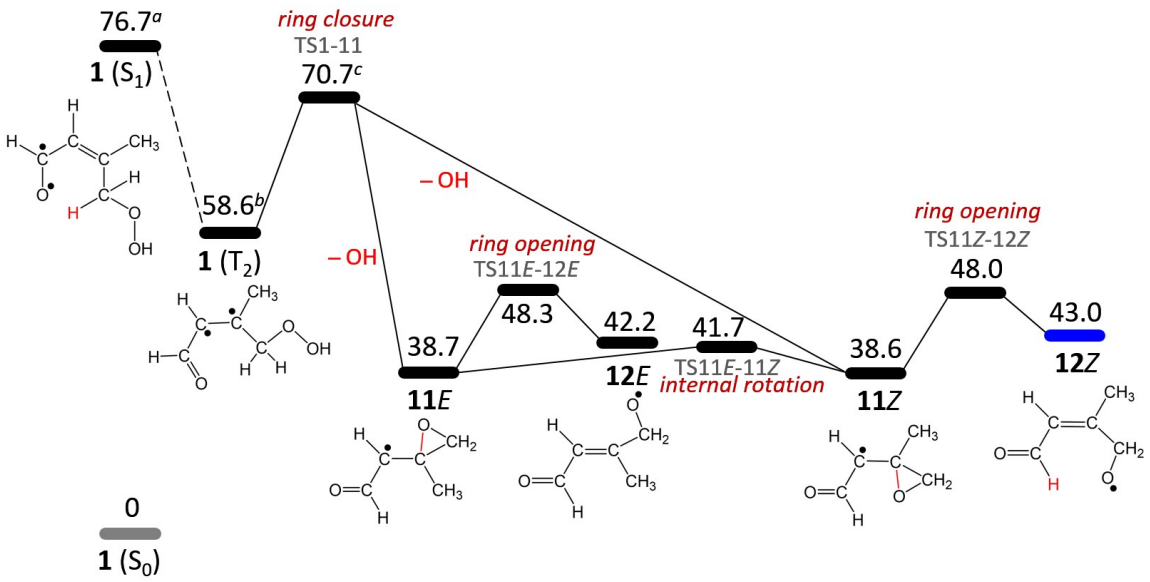

Figure 3a. Potential energy surface for the reactions of the excited HPALD(II) through triplet (T_2) state. Coupled-cluster energies (kcal mol^{-1}) relative to the global minimum singlet *Z*- HPALD(II) and the corresponding fragment OH, based on DFT geometries (CCSD(T)-F12/cc-pVDZ-F12//M06-2X-D3/6-311++G(2d,p) level of theory). ZPVE at M06-2X-D3/6-311++G(2d,p) level is included. [a] For the excited **1**, the TD-M06-2X-D3 energy is shown. [b] The relative energy is shown for the lowest reactive *Z*- HAPLD(II) out of 12 reactive conformers (or 29 conformers in total, see Figure S4 in the ESI). [c] The relative energy is shown for the lowest transition state out of 8 transition states in total, see Figure S5 in the ESI. Other structures are depicted in the ESI (Figure S6).

states $N_i(E)$ and equal to $P_i = N_i(E)/\Sigma_i N_i(E)$, with $\Sigma_i N_i(E)$ over all conformers. In terms of RRKM theory, the overall energy-specific rate coefficient is then given by $k(E) = (1/h)\,\Sigma_j\{P_j \times G^{\neq}_j/N_j\} = (1/h)\,\Sigma_j G^{\neq}_j/\Sigma_i N_i$, with P_j and N_j referring to the 12 reactive conformers and the sums of accessible states $G^{\neq}_j$ to the TSs through which they react, the numerator sum taken over the 12 reactive conformers, and the denominator sum over all 29 conformers. The $k(E)$ was computed over the $F(E_{exc})$ range from E_{exc} = 78 to 104 kcal mol^{-1}.

At the median excitation energy of 89 kcal mol^{-1} $k(E)$ = 1.2 × 10^9 s^{-1}, which implies that collisional energy loss and stabilization will be competitive, in particular at the lower excitation energies. An RRKM-Master Equation analysis was therefore performed, adopting an average energy transfer per collision with air molecules of $\langle\Delta E\rangle$ = -200 cm^{-1}, and a collision frequency at 1 atm and 298 K of 1.3 × 10^{10} s^{-1}. As expected for a case where a large amount of energy, about 30 kcal mol^{-1} on average, has to be lost before stabilization, requiring a very large number of collisions, the calculated fraction of collisional stabilization, averaged over the excitation distribution $F(E_{exc})$, was quasi identical for a model with a fixed energy of 200 cm^{-1} transferred per collision as for a bi-exponential type model with the same average energy transferred, both models yielding 0.56. Table S3 lists the microcanonical rate coefficient $k(E)$ and the fractional reaction yield $f_{react}(E)$ of T_2 as a function of the initial excitation energy *E* for HPALD(II). Thus, for HPALD(II) the fraction T_2 reacting to OH + **11** was found to be 0.44. For HPALD(I), the fraction calculated in a similar way is 0.52. It is likely that some additional OH may be produced by a similar mechanism from the peroxy radical resulting from the stabilized T_2, as the O_2-addition leaves some 26 kcal mol^{-1} internal energy in that molecule; however, this mechanism will not be further explored here. In any case, the O_2 addition to stabilized T_2 has to compete with its ISC to S_0 , of which the rate may be estimated at *ca.* 10^7 s^{-1} by analogy with 2-butene.[38] Such a relatively slow $T_2 \rightarrow S_0^{\dagger}$ ISC should also preclude an important contribution of the impulsive dissociation of activated $S_0^{\dagger}$ from this process into OH + enoxy radical.

A second important issue regarding the $T_2 \rightarrow$ OH + **11** reaction is the disposal of the potential energy decrease

View Article Online
DOI: 10.1039/C7CP00288B

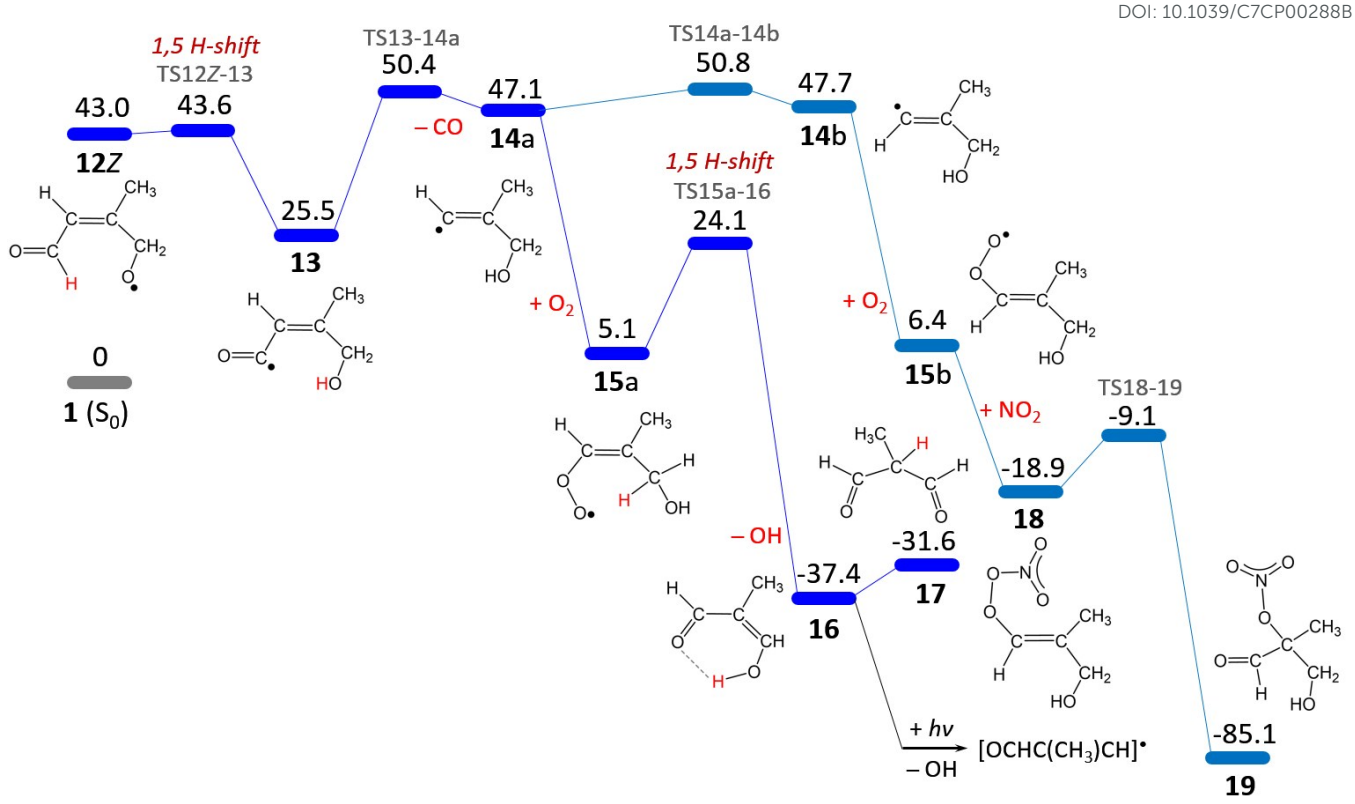

Figure 3b. Potential energy surface for the following reactions from 12*Z*. Coupled-cluster energies (kcal mol^{-1}) relative to the global minimum singlet *Z*- HPALD(II) and the corresponding fragments OH, OOH and O_2, based on DFT geometries (CCSD(T)-F12/cc-pVDZ-F12//M06-2X-D3/6-311++G(2d,p) level of theory). All structures are depicted in the ESI (Figure S6).

from the TS to the products, of about 32 kcal mol^{-1} (see Figure 3a and Table 2). An intrinsic reaction coordinate analysis (IRC) reveals that during this decrease the O8 oxygen atom barely moves relative to the center of mass — except for the last few kcal mol^{-1} of this decrease to allow the full development of the –O7–HO8 hydrogen bond of the product complex — while the most important geometry change is the continued approach of O7 to C3. The potential energy decrease which is due to the formation of the new, ~60 kcal mol^{-1} strong O7–C3 bond will therefore end up predominantly in vibration of that bond and of oxirane-ring deformation. Eventually, a small fraction of the total internal energy of the product complex goes to breaking the 4 – 5 kcal mol^{-1} H-bond. Assuming equipartition over all degrees of freedom of the separating fragments **11** and O8H, a fraction ~36/42 of the average ~50 kcal mol^{-1} disposable energy of the complex should go to the **11** fragment, i.e. some 43 kcal mol^{-1}. This should be a conservative estimate as the average initial energy of the reacting fraction of T_2 is several kcal mol^{-1} higher than the overall average adopted here (see Table S3). The hot product radical arising as both **11***Z*- and **11***E*-isomer, promptly opens the oxirane-ring over a barrier of only ~10 kcal mol^{-1} (see Figure 3a) to form various conformers of the chemically activated *Z*- and *E*- O6=C1H-C2H=C3(C_5H_3)-$C4H_2$-O7$^\bullet$ enoxy radicals **12***Z* and **12***E*. As reported earlier,[39] these two isomeric forms can readily interconvert by reverting promptly to **11** followed by internal rotation about the C2—C3 bond over a low barrier of 3 kcal mol^{-1}.

Fate of the enoxy radicals from HPALDs. As shown in Figure 3b, and referring to the energy data listed in Table 2, the predominant and fast sink of the hot enoxy radical pool is the spontaneous, quasi-barrierless and exothermic 1,5 H-shift in *Z*- enoxy **12***Z* of the formyl-H to the oxy site, forming *Z*- O6=C1$^\bullet$-C2H=C3(C_5H_3)-$C4H_2$-O7H radicals, with nascent internal energy of some 55 kcal mol^{-1}. For HPALD(I), there is in principle another sink, a 1,5 H-shift in the *E*- enoxys of a methyl-H to the oxy radical site, but this process faces a barrier of 10.0 kcal mol^{-1} and can

View Article Online
DOI: 10.1039/C7CP00288B

Table 2: Relative energies and free energies (kcal mol^{-1}) at 298 K for the structures in Figure 3a and Figure 3b.

	$\nu_{im}^{\neq}$/i	ΔE_1	ΔG_1 (298 K)	ΔE_2	ΔG_2 (298 K)
11*E*		37.5	28.2	38.7	29.4
TS11*E*-12*E*	-582	51.1	41.4	48.3	38.7
12*E*		42.5	32.2	42.2	31.9
TS11*E*-11*Z*	-96	41.0	32.0	41.7	32.8
11*Z*		37.4	27.9	38.6	29.1
TS11*Z*-12*Z*	-591	50.7	41.3	48.0	38.6
12*Z*		42.9	32.6	43.0	32.7
TS12*Z*-13	-544	45.1	35.6	43.6	34.1
13		26.3	16.4	25.5	15.6
TS13-14a	-312	51.9	40.8	50.4	39.3
14a		49.6	29.5	47.1	27.0
15a		6.7	-2.4	5.1	-4.1
TS15a-16	-1760	27.0	18.2	24.1	15.3
16		-32.7	-50.8	-37.4	-55.5
17		-25.4	-44.5	-31.6	-50.7
TS14a-14b	-719	53.4	33.3	50.8	30.6
14b		50.6	30.4	47.7	27.5
15b		7.7	-2.1	6.4	-3.4
18		-17.4	-14.8	-18.9	-16.3
TS18-19	-415	-4.2	-1.3	-9.1	-6.2
19		-84.4	-81.1	-85.1	-81.8

ΔE_1, the relative energy with inclusion of ZPVE at M06-2X-D3/6-311++G(2d,p) level of theory; ΔG_1, the relative Gibbs free energy at M06-2X-D3/6-311++G(2d,p) level of theory; ΔE_2, the relative energy with inclusion of ZPVE at CCSD(T)-F12/cc-pVDZ-F12//M06-2X-D3/6-311++G(2d,p) level of theory; ΔG_2, the relative Gibbs free energy at CCSD(T)-F12/cc-pVDZ-F12//M06-2X-D3/6-311++G(2d,p) level of theory; $\nu_{im}^{\neq}$/i, the imaginary frequency of the TSs.

therefore account for no more than 20% of the enoxy removal rate, and only for HPALD(I). The hot *Z*- O6=C1$^{\bullet}$-C2H=C3($C5H_3$)-$C4H_2$-O7H radicals will promptly eliminate CO over a barrier of 24.9 kcal mol^{-1} at an RRKM-calculated rate of 1.3 × 10^{10} s^{-1}, outrunning collisional stabilization. The resulting $^{\bullet}$C2H=C3($C5H_3$)-$C4H_2$-O7H radicals arise as structure **14**a, with the H-atom on C2 in *trans* to the -CH2OH group, but can isomerize to the *cis*-structure **14**b over a barrier of only 3.7 kcal mol^{-1} resulting, after collisional thermalization, in a fast pre-equilibrium with ratio **14**a : **14**b of 1 : 0.36. Both will quickly add O_2, forming the *Z*- and *E*- $^{\bullet}$OO-C2H=C3($C5H_3$)-$C4H_2$-O7H vinylic peroxy radicals **15**a and **15**b in the same ratio. The *Z*-vinylic peroxys undergo a 1,5 H-shift of an α-hydrogen from the alcohol function to the peroxy site over a barrier of 19.0 kcal mol^{-1} at a thermal rate of 7 s^{-1} (with tunneling factor of 195 for $\nu^{\neq}_{im}$ = 1740 cm^{-1}) forming the unstable *Z*-HOO-C2H=C3($C5H_3$)-C4$^{\bullet}$H-O7H ↔ HOO-$^{\bullet}$C2H-C3($C5H_3$)=C4H-O7H radical that spontaneously expels OH without barrier to generate hydroxy-methacrolein O=C2H-C3($C5H_3$)=C4H-O7H **16**.

The latter is stabilized by a non-classical ≈10 kcal mol^{-1} strong H-bond and shows aromatic character, such that its free energy at 298 K is 4.7 kcal mol^{-1} below that of its β-dicarbonyl tautomer, 2-formyl-propanal **17**. This behavior is similar to that of the analogous ketone-enol tautomer of acetylacetone, which is known to exhibit a high near-UV absorption cross section for the (allowed!) π,π* transition.[40] Again by analogy with the tautomer of acetylacetone, hydroxy-methacrolein **16** should therefore photolyze quickly into OH and a strongly resonance-stabilized radical[41] at a rate estimated at about (2 - 3) × 10^{-4} s^{-1} for an overhead sun using the absorption cross sections for acetylacetone[40] and assuming a quantum yield of unity. However, similar to the tautomer of acetylacetone, the aldehyde-enol is expected to react also very quickly with OH, with a rate coefficient close to 1 × 10^{-10} cm^3 s^{-1}.[42] The net OH budget of the chemistry of *Z*-enoxy **12***Z* is therefore uncertain, and may be decided by the (unknown) subsequent chemistry of the [OCHC(CH_3)CH]$^{\bullet}$ photo-product radical and of the OH-adducts.

For the *E*- vinylic peroxy radicals **15**a, a fast H-shift is not possible and their fate should be reactions with NO, HO_2 or RO_2, though most interestingly, another and faster pathway is open to these radicals: they can irreversibly add NO_2 followed by a prompt, newly characterized isomerization process to quickly yield an hydroxy-carbonylnitrate, shown in Figure 3b. The radical-radical combination of the vinylic peroxy **15**a with NO_2 leads first to a vinylic peroxynitrate **18**, but while alkylperoxynitrates which are stable by only around 20 kcal mol^{-1} merely redissociate within a fraction of a second, this vinylic peroxynitrate isomerises much faster over a barrier of only 9.8 kcal mol^{-1} through a fairly loose TS to form a carbonyl-nitrate **19** that is 66.2 kcal mol^{-1} more stable. For an internal energy of 29 kcal mol^{-1}, the calculated prompt rate of rearrangement of **18** is 9.1 × 10^9 s^{-1}, far faster than

View Article Online
DOI: 10.1039/C7CP00288B

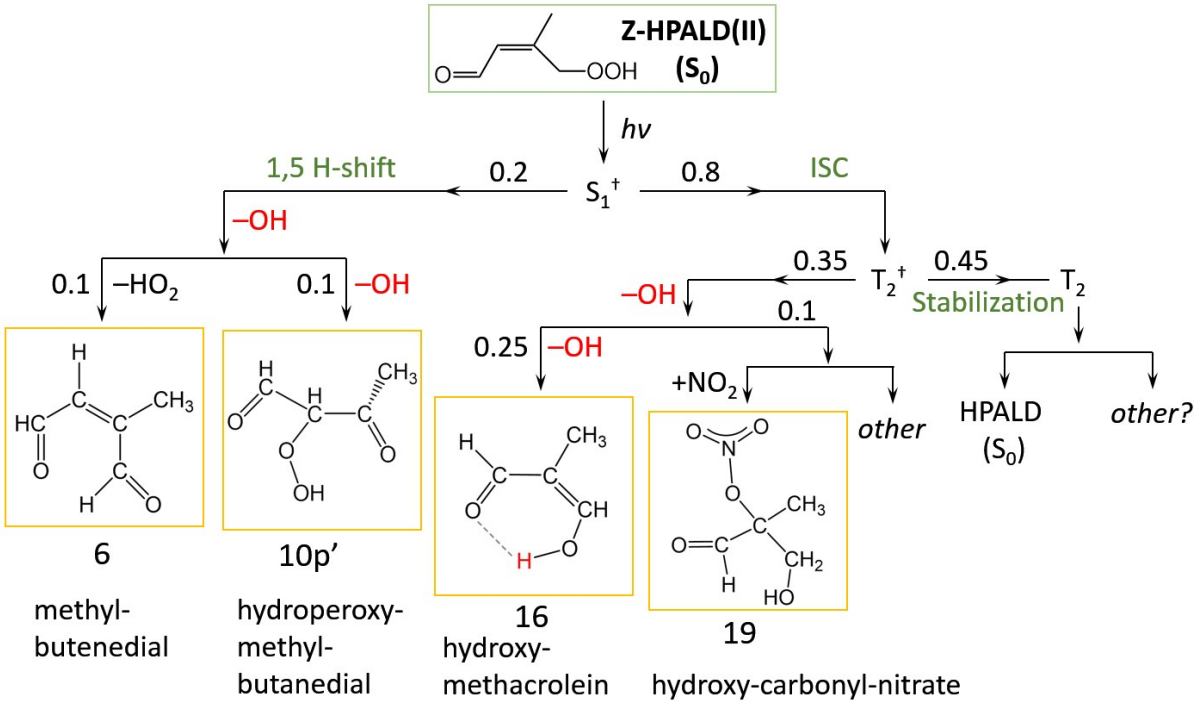

Figure 4. Flowchart of HPALD photolysis mechanisms quantified in this work. The numbers give the estimated overall branching fractions.

its collisional stabilization. Anyway, the thermal reaction at rate 2.4 × 10^5 s^{-1} will also outrun any competing process. Up to 9% of the excited HPALD(II) may be channeled through this newly predicted pathway which may contribute substantially to nitrate formation from isoprene. Interestingly, the hydroxy-carbonyl-nitrates expected here are the same as the major carbonyl-nitrates produced in the oxidation of isoprene at high NO[43] and that were recently argued to undergo rapid photolyis.[44]

Overall Quantum yields of HPALD photolysis and of OH formation. As summarized in Figure 4, the quantum yield of HPALD(II) photolysis can be estimated at *ca.* 0.20 from the S_1 mechanism plus 0.35 from the T_2 mechanism, or an overall QY of *ca.* 0.55. For HPALD(I) the photolysis quantum yield is similar, *ca.* 0.13 from the S_1 mechanism and 0.45 from T_2. The quantum yield of first-generation OH production depends for a part on follow-up radical chemistry and is therefore harder to evaluate; for the first mechanism of HPALD(II) it was estimated above at around 0.3, while for the second mechanism — with a branching ratio to the *Z*- and *E*- vinylic peroxys of 1 : 0.36, about 0.6 OH is expected, for a total QY(OH) of *ca*. 0.9. This result can be compared with the QY(OH) of 1 ± 0.8 measured by Wolfe et al.[12] for the HPALD proxy *Z*- O=CH-CH=CH-CH(OOH)C_2H_5.

Conclusions and atmospheric implications

In this work we proposed and theoretically quantified two efficient mechanisms for the atmospheric photolysis of *Z*- HPALDs. Both these mechanisms involve molecular rearrangements of excited state HPALDs before the release of OH. The flowchart in Figure 4 presents the various reaction steps or reaction sequences in the photolysis mechanism that result in the 1st-generation products and also gives the overall branching fractions; the overall OH quantum yield is the sum of the pertaining branching fractions. We showed that, as a first mechanism, specific conformers of the initially formed S_1 state promptly undergo a nearly barrierless 1,5 H-shift on a picosecond time-scale that competes effectively with the very fast ISC to the triplet T_2 state, followed in a second step by a prompt and likewise quasi-barrierfree expulsion of an hydroxyl radical. The highly stabilized co-product radical partly yields a second hydroxyl in a sequence of unimolecular reactions. As a second

mechanism, we newly identified a prompt reaction of the activated triplet T_2 state involving concerted expulsion of OH and oxirane ring formation, in competition with collisional stabilization. The 3-membered cyclic co-product radical was found to convert quickly to an enoxy radical of which the subsequent chemistry leads for the larger part to another OH radical. The two mechanisms result in an overall photolysis quantum yield of ≈0.55, while the quantum yield of OH-production is ≈0.9.

The second, most important mechanism was already anticipated in our earlier paper on the LIM1 mechanism.[8] The proposed subsequent chemistry could be confirmed at present and the pertaining barrier heights and reaction rates upgraded and refined. On the other hand, the originally proposed mechanism of HPALD photolysis, involving an avoided crossing of the S_1 surface and a repulsive RO--OH singlet state[11] had to be abandoned on account of a too-high lying reaction bottleneck. Nevertheless, the products of that process are the same as formed indirectly, in the present second mechanism, through the T_2 state. Regarding the presently predicted quantum yields of photolysis and hydroxyl formation, the true values might be significantly higher, since it cannot be excluded that other parallel photolysis routes have been overlooked here, among others a mechanism involving the peroxy radical from the collisionally stabilised T_2 state, though that particular route is likely to be less important.

This OH quantum yield of 0.9 is well in line both with our previous theoretical expectation[11] and with the experimental QY(OH) for a HPALD proxy,[12] confirming the significant role of HPALD as secondary OH source over isoprene-rich areas. Although second-generation OH production is expected from the photolysis of the hydroperoxy-dials (**10p** and **10p'**), the precise overall impact of HPALD photolysis on OH remains difficult to quantify as it will depend on the further chemistry of the products, most importantly hydroxy-methacrolein.

Our estimated overall photolysis quantum yield (≥0.55) is compatible with the experimental QY range.[12] It is worth noting that a low value (≈0.55) would imply an upward revision of the HPALD photolysis lifetime, by almost a factor of 2 compared to model estimates assuming a unit quantum yield.[11,14,45-47] This could partly explain the noted underestimation of calculated HPALD concentrations against aircraft measurements in a recent modelling study.[14]

The formation of carbonyl nitrates from the reactions of *E*- vinylic peroxy radicals (**15a**) with NO_2 is a likely significant source of atmospheric organic nitrates, estimated here at *ca*. 0.5 TgN yr^{-1} (adopting a 15% HPALD average yield from isoprene+OH[14] and assuming that photolysis accounts for about two thirds of HPALD sink and 50% of the vinyl peroxys react with NO_2), to be compared with the production of hydroxynitrates from the reactions of ISOPO2 with NO, estimated at *ca*. 4 TgN yr^{-1} (assuming that 40% of ISOPO2 react with NO, and adopting a 10% nitrate yield[45] in the reaction). Nevertheless, the contribution of those carbonyl nitrates to the total alkyl nitrate burden should be small, given their very short atmospheric lifetimes, of the order of one hour during daytime in the case of the nitroxy aldehyde **19**.[44]

Acknowledgements

This work was sponsored in part by Belspo under contract SD/CS/05A (project BIOSOA) in the frame of the Science for Sustainable Development program. It also received support from project PRODEX ACROSAT of the European Space Agency funded by the Belgian Science Policy Office (Belspo), and the grant #C14/15/052, by the KU Leuven.

References

1 A. B. Guenther, X. Jiang, C. L. Heald, T. Sakulyanontvittaya, T. Duhl, L. K. Emmons, and X. Wang, *Geosci. Model Dev.,* 2012, **5**, 1471-1492.
2 J. Lelieveld, T. M. Butler, J. N. Crowley, T. J. Dillon, H. Fischer, L. Ganzeveld, H. Harder, M. G. Lawrence, M. Martinez, D. Taraborrelli, and J. Williams, *Nature,* 2008, **452**, 737-740.
3 A. Hofzumahaus, F. Rohrer, K. Lu, B. Bohn, T. Brauers, C. C. Chang, H. Fuchs, F. Holland, K. Kita, Y. Kondo, X. Li, S. Lou, M. Shao, L. Zeng, A. Wahner, and Y. Zhang, *Science,* 2009, **324**, 1702-1704.
4 J. Peeters, T. L. Nguyen, and L. Vereecken, *Phys. Chem. Chem. Phys.,* 2009, **11**, 5935-5939.
5 F. Paulot, J. D. Crounse, H. G. Kjaergaard, A. Kurtèn, J. M. St. Clair, J. H. Seinfeld, and P. O. Wennberg, *Science,* 2009, **325**, 730-733.
6 J. D. Crounse, H. C. Knap, K. B. Ørnso, S. Jørgensen, F. Paulot, H. G. Kjaergaard, and P. O. Wennberg, *J. Phys. Chem. A,* 2012, **116**, 5756-5762.

7 E. Praske, J. D. Crounse, K. H. Bates, T. Kurtén, H. G. Kjaergaard, and P. O. Wennberg, *J. Phys. Chem. A,* 2015, **119**, 4562-4572.
8 J. Peeters, J.-F. Müller, T. Stavrakou, and V. S. Nguyen, *J. Phys. Chem. A,* 2014, **118**, 8625-8643.
9 H. Fuchs, A. Hofzumahaus, F. Rohrer, B. Bohn, T. Brauers, H. P. Dorn, R. Häseler, F. Holland, M. Kaminski, X. Li, K. Lu, S. Nehr, R. Tillmann, R. Wegener, and A. Wahner, *Nat. Geosci.,* 2013, **6**, 1023-1026.
10 J. Lelieveld, S. Gromov, A. Pozzer, and D. Taraborrelli, *Atmos. Chem. Phys.,* 2016, **16**, 12477-12493.
11 J. Peeters, and J.-F. Müller, *Phys. Chem. Chem. Phys.,* 2010, **12**, 14227-14235.
12 G. M. Wolfe, J. D. Crounse, J. D. Parrish, J. M. St. Clair, M. R. Beaver, F. Paulot, T. P. Yoon, P. O. Wennberg, and F. N. Keutsch, *Phys. Chem. Chem. Phys.,* 2012, **14**, 7276-7286.
13 J. D. Crounse, F. Paulot, H. G. Kjaergaard, and P. O. Wennberg, *Phys. Chem. Chem. Phys.,* 2011, **13**, 13607-13613.
14 K. R. Travis, D. J. Jacob, J. A. Fisher, P. S. Kim, E. A. Marais, L. Zhu, K. Yu, C. C. Miller, R. M. Yantosca, M. P. Sulprizio, A. M. Thompson, P. O. Wennberg, J. D. Crounse, J. M. St. Clair, R. C. Cohen, J. L. Laughner, J. E. Dibb, S. R. Hall, K. Ullmann, G. M. Wolfe, I. B. Pollack, J. Peischl, J. A. Neuman, and X. Zhou, *Atmos. Chem. Phys.,* 2016, **16**, 13561-13577.
15 J. W. Ponder, and F. M. Richards, *J. Comput. Chem.*, 1987, **8**, 1016-1024.
16 Gaussian 09, Revision E.01, M. J. Frisch, G. W. Trucks, H. B. Schlegel, G. E. Scuseria, M. A. Robb, J. R. Cheeseman, G. Scalmani, V. Barone, B. Mennucci, G. A. Petersson, H. Nakatsuji, M. Caricato, X. Li, H. P. Hratchian, A. F. Izmaylov, J. Bloino, G. Zheng, J. L. Sonnenberg, M. Hada, M. Ehara, K. Toyota, R. Fukuda, J. Hasegawa, M. Ishida, T. Nakajima, Y. Honda, O. Kitao, H. Nakai, T. Vreven, J. A. Montgomery, Jr., J. E. Peralta, F. Ogliaro, M. Bearpark, J. J. Heyd, E. Brothers, K. N. Kudin, V. N. Staroverov, R. Kobayashi, J. Normand, K. Raghavachari, A. Rendell, J. C. Burant, S. S. Iyengar, J. Tomasi, M. Cossi, N. Rega, J. M. Millam, M. Klene, J. E. Knox, J. B. Cross, V. Bakken, C. Adamo, J. Jaramillo, R. Gomperts, R. E. Stratmann, O. Yazyev, A. J. Austin, R. Cammi, C. Pomelli, J. W. Ochterski, R. L. Martin, K. Morokuma, V. G. Zakrzewski, G. A. Voth, P. Salvador, J. J. Dannenberg, S. Dapprich, A. D. Daniels, Ö. Farkas, J. B. Foresman, J. V. Ortiz, J. Cioslowski, and D. J. Fox, Gaussian, Inc., Wallingford CT, 2009.
17 (a) H.-J. Werner, P. J. Knowles, G. Knizia, F. R. Manby, and M. Schütz, *WIREs Comput. Mol. Sci.*, 2012, **2**, 242-253. (b) MOLPRO, version 2012.1, a package of ab initio programs, H.-J. Werner, P. J. Knowles, G. Knizia, F. R. Manby, M. Schütz, and others, see http://www.molpro.net.
18 W. Forst, Theory of Unimolecular Reactions, Academic Press, New York, 1973.
19 K.A. Holbrook, M.J. Pilling, and S.H. Robertson, Unimolecular Reactions (2nd ed.), John Wiley & Sons, New York, 1996.
20 L. Vereecken, and J. Peeters, *J. Chem. Phys.,* 2003, **119**, 5159-5170.
21 H. S. Johnston, and J. Heicklen, *J. Phys. Chem.,* 1962, **66**, 532-533.
22 M. L. Coote, M. A. Collins, and L. E. O. Radom, *Mol. Phys.,* 2003, **101**, 1329-1338.
23 R. C. Raid, J. M. Prausnitz, and T. K. Sherwood, The Properties of Gases and liquids, McGrawHill, New York, 1977.
24 J. Troe, *J. Chem. Phys.,* 1977, **66**, 4745-4757.
25 J. D. Crounse, A. Teng, and P. O. Wennberg, Experimental constraints on the distribution and fate of peroxy radicals formed in reactions of isoprene + OH + O_2, ACM Meeting, Davis, CA, Dec. 2014.
26 T. Gierczak, J. B. Burkholder, R. K. Talukdar, A. Mellouki, S. B. Barone, and A. R. Ravishankara, *J. Photochem. Photobiol. A: Chem.,* 1997, **110**, 1-10.
27 S. Madronich, UV radiation in the natural and perturbed atmosphere, in Environmental Effects of Ultraviolet Radiation, edited by M. Tevini, pp. 17-69, Lewis, Boca Raton, Florida, 1993.
28 A. D. Walsh, *Trans. Faraday Soc.,* 1945, **41**, 498-505.
29 M. Reguero, M. Olivucci, F. Bernardi, and M. A. Robb, *J. Am. Chem. Soc.,* 1994, **116**, 2103-2114.
30 K. W. Paulisse, T. O. Friday, M. L. Graske, and W. F. Polik, *J. Chem. Phys.,* 2000, **113**, 184-191.
31 W.-H. Fang, *J. Am. Chem. Soc.,* 1999, **121**, 8376-8384.
32 L. Vereecken, T. L. Nguyen, I. Hermans, and J. Peeters, *Chem. Phys. Lett.,* 2004, **393**, 432-436.
33 L.P. Thüner, G. Rea, and J.C. Wenger, Photolysis of Butenedial and 4-Oxopent-2-enal, in I. Barnes (eds). The European Photoreactor EUPHORE 4th Report. Wuppertal, Germany: University of Wuppertal, 2003.
34 J. Peeters, and T. L. Nguyen, *J. Phys. Chem. A,* 2012, **116**, 6134-6141.
35 K. T. Kuwata, A. S. Hasson, R. V. Dickinson, E. B. Petersen, and L. C. Valin, *J. Phys. Chem. A,* 2005, **109**, 2514-2524.
36 R. Asatryan, G. da Silva, and J. W. Bozzelli, *J. Phys. Chem. A,* 2010, **114**, 8302-8311.
37 S. Jørgensen, H. C. Knap, R. V. Otkjaer, A. M. Jensen, M. L. H. Kjeldsen, P. O. Wennberg, and H. G. Kjaergaard, *J. Phys. Chem. A,* 2016, **120**, 266-275.
38 B. Singh, and E. F. Ullman, *J. Am. Chem. Soc.,* 1967, **89**, 6911-6916.
39 V. S. Nguyen, and J. Peeters, *J. Phys. Chem. A,* 2015, **119**, 7270-7276.
40 H. Nakanishi, H. Morita, and S. Nagakura, *Bull. Chem. Soc. Jpn.,* 1977, **50**, 2255-2261.
41 M.-C. Yoon, Y. S. Choi, and S. K. Kim, *Chem. Phys. Lett.,* 1999, **300**, 207-212.
42 S. Zhou, I. Barnes, T. Zhu, I. Bejan, M. Albu, and T. Benter, *Environ. Sci. Technol.,* 2008, **42**, 7905-7910.
43 F. Paulot, J. D. Crounse, H. G. Kjaergaard, J. H. Kroll, J. H. Seinfeld, and P. O. Wennberg, *Atmos. Chem. Phys.,* 2009, **9**, 1479-1501.
44 J.-F. Müller, J. Peeters, and T. Stavrakou, *Atmos. Chem. Phys.,* 2014, **14**, 2497-2508.
45 A. Archibald, M. C. Cooke, S. R. Utembe, D. Shallcross, R. G. Derwent, and M. E. Jenkin, *Atmos. Chem. Phys.*, 2010, **10**, 8097-8118.
46 M. E. Jenkin, J. C. Young, and A. R. Rickard, *Atmos. Chem. Phys.*, 2015, **15**, 11433-11459.
47 C. Chan Miller, D. J. Jacob, E. A. Marais, K. Yu, K. R. Travis, P. S. Kim, J. A. Fisher, L. Zhu, G. M. Wolfe, F. N. Keutsch, J. Kaiser, K.-E. Min, S. S. Brown, R. A. Washenfelder, G. Gonzàlez Abad, and K. Chance, *Atmos. Chem. Phys. Discuss.*, 2016, doi:10.5194/acp-2016-1042, in review.